Aeroelastic Optimization of a 10 MW Wind Turbine Blade with Active Trailing Edge Flaps

Thanasis K. Barlas[*] Carlo Tibaldi[†] Frederik Zahle[‡] Helge Madsen[§]

Technical University of Denmark (DTU), Wind Energy Department, 4000 Roskilde, Denmark

This article presents the aeroelastic optimization of a 10MW wind turbine 'smart blade' equipped with active trailing edge flaps. The multi-disciplinary wind turbine analysis and optimization tool HawtOpt2 is utilized, which is based on the open-source framework Open-MDAO. The tool interfaces to several state-of-the art simulation codes, allowing for a wide variety of problem formulations and combinations of models. A simultaneous aerodynamic and structural optimization of a 10 MW wind turbine rotor is carried out with respect to material layups and outer shape. Active trailing edge flaps are integrated in the design taking into account their achieved fatigue load reduction. The optimized 'smart blade' design is compared to an aeroelastically optimized design with no flaps and the baseline design.

I. Introduction

The size of wind turbines has been increasing rapidly over the past years. Rotors of more than 160m in diameter are already commercially available. Focusing on lowering the cost per kWh, new trends and technological improvements have been primary targets of research and development. One main focus is on developing new technologies, which are, amongst other, capable of considerably reducing fatigue loads on wind turbines. New concepts for dynamic load reduction are focusing on a much faster and detailed load control, compared to existing individual blade pitch control, by utilizing active aerodynamic control devices distributed along the blade span.[1] Such concepts are generally referred to as smart rotor control, a term used in rotorcraft research, and investigated for wind turbine applications over the past years in terms of conceptual and aeroelastic analysis, small scale wind tunnel experiments, and recently field testing.[2,3] For a review of the state-of-the-art in the topic, the reader is referred to.[1] So far, results from numerical and experimental analysis mostly focusing on trailing edge flaps have shown a considerable potential in fatigue load reduction.[4,8] Existing work has focused on application of active flaps on existing blade designs,[5–7] implicitly showing the potential for reduction of cost of energy, however the potential of a fully redesigned and optimized blade integrating the use of active flaps has not yet been explored.

In the recent years several frameworks have been present to perform wind turbine multi-disciplinary optimization design.[10–15] In this work an optimization framework named HawtOpt2 is utilized which enables concurrent optimization of the structure and outer shape of a wind turbine blade. This tool builds on the experience gained with the HawtOpt code[9] but is otherwise a completely new codebase written in the Python programming language, and based on the open source framework OpenMDAO[19] which is used to define the optimization problem, and handle the data and workflow. Different tools have been interconnected within the framework to resolve the different levels of the problem. The finite element cross sectional tool BECAS[25] is used to predict the structural and mass properties and to retrieve stresses along the blades. The aeroservoelastic tool HAWCStab2[26] is used to predict aerodynamic performance and deflections of the

---

[*]Researcher, Aeroelastic Design Group, Wind Energy Department, Technical University of Denmark, Fredriksborgvej 399, 4000 Roskilde, Denmark.

[†]Post-Doc Researcher, Aeroelastic Design Group, Wind Energy Department, Technical University of Denmark, Fredriksborgvej 399, 4000 Roskilde, Denmark.

[‡]Senior Researcher, Aeroelastic Design Group, Wind Energy Department, Technical University of Denmark, Fredriksborgvej 399, 4000 Roskilde, Denmark.

[§]Professor, Aeroelastic Design Group, Wind Energy Department, Fredriksborgvej 399, 4000 Roskilde, Denmark.

rotor, modal properties of the turbine, and retrieve a linearized model of the turbine. A method to evaluate fatigue damage loads in the frequency domain is also used.[17,18]

The overall objective of the paper is to apply the developed aeroelastic optimization framework on the design of a blade incorporating active trailing edge flaps. An example layout of the blade planform incorporating passive (fixed) and active trailing edge flap sections in shown in Figure 1. The added value of the optimized 'smart blade' design is thus shown through a comparison to an aeroelastically optimized design with no flaps and a baseline design.

The overall idea in the blade design with trailing edge flaps is that the blade is designed and manufactured without the trailing edge part (e.g. 10% of the chord) over the whole span. On the inboard part flat back airfoils are used and further outboard the flaps are mounted in a combination of active and passive flaps. The active flaps have a constant chord as they are manufactured in an extrusion process. The passive flaps are mold manufactured and have a full 3D outer shape are are thus used between the active flaps to achieved the desired spanwise variation of the blade planform.

II.   Aeroelastic optimization framework and models

The HawtOpt2 framework is used in this work in a similar fashion as described in.[16] The HawtOpt2 framework uses OpenMDAO (Open-source Multidisciplinary Design, Analysis, and Optimization Framework)[19] to handle the definition of the optimization problem, workflow, dataflow and parallelization of simulation cases. In this work, the gradient-based sequential quadratic programming optimizer SNOPT[20,21] is used. The development of the HawtOpt2 framework is part of a larger effort named Framework for Unified Systems Engineering and Design of Wind Turbine Plants (FUSED-Wind).[22]

Interfaces have been developed to connect the optimization framework to the finite element cross sectional tool BECAS and to the aeroelastic tool HAWCStab2, that form the core of the state-of-the art analysis capability provided by the tool. BECAS[23–25] allows for the evaluation of the cross sectional structural and mass properties of the blade. The tool is based on a 2D finite element formulation that allows for an exact geometrical description of the section. Different regions with different material and different thicknesses can be specified enabling the description of different layups. The linear high-order aeroservoelastic model implemented in HAWCStab2[26–29] uses an unsteady blade element momentum (BEM) model of the rotor and a geometrically nonlinear finite beam element model to compute steady-state aerodynamic states, structural deflections, and linearized models of the wind turbine.

A method to evaluate fatigue damage based on a linear model is also used. The method is frequency-domain based and it does therefore not require time-domain simulations. This peculiarity is central for gradient-based optimization since the stochastic nature of time-domain simulations with turbulence does not allow for accurate evaluation of gradients of objectives and constraints with respect to the design variables. The method is described in detail by Tibaldi et al.[18] Furthermore, the effect of the trailing edge flaps in the linear
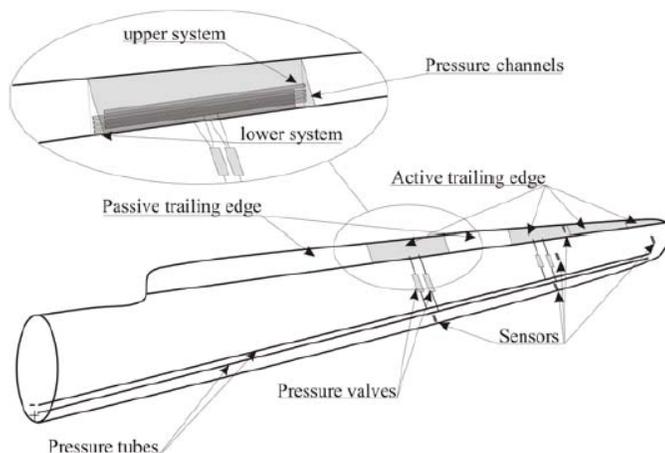

Figure 1. Blade planform geometry incorporating passive (fixed) and active trailing edge flap sections

American Institute of Aeronautics and Astronautics

aeroelastic model is integrated based on.[30] In this implementation, a quasi-steady aerodynamic trailing edge flap model is utilized, which provides the effect of an individual flap controller on the fatigue load estimation.

III. Blade parametrization

To enable optimization of both the structure and aerodynamic shape of the blade, a suitable parameterization of the geometry is chosen, utilizing the so-called free-form deformation (FFD) splines based on Bezier curves. The blade planform is described in terms of distributions of chord, twist, relative thickness, and pitch axis aft leading edge. In addition, the flap spanwise extent is defined. The lofted shape of the blade is generated based on interpolation of a family of airfoils with different relative thicknesses, see Fig. 2. The internal structure is defined from a number of regions that each cover a fraction of the cross-sections along the blade. Each region consists of a number of materials that are placed according to a certain stacking sequence. Figure 2 shows a cross section in which the region division points (DPs) are indicated. The DP curves are described by a smooth spline as function of span that takes values between s=-1 and s=1, where s=-1 is located at the pressure side trailing edge, s=0 is at the leading edge, and s=1 is located at the trailing edge suction side. Shear webs are associated to two specific DPs on the pressure and suction side, respectively, and will move according to these points. To facilitate the flap integration, all blade sections are defined with a flatback trailing edge, allowing for a 10% chordwise percentage of flapped section. The flapped trailing edge section is passive (fixed) on all spanwise sections except the ones involving the active flap geometry.

The composite layup is likewise delineated by a series of smooth splines describing the thicknesses of individual layers. Figure 3 shows the composite layup of the DTU 10MW RWT for regions 0 to 6. Note that the layup of the DTU 10MW RWT has the same material distributions on the suction and pressure sides. Also indicated in Figure 3 are the materials in the blade, which in this work are included as design variables. This includes both uniax and triax material in the trailing edge, biax in the trailing panel, uniax in the spar caps, and triax and uniax in the leading edge panels. As for the baseline design, all material thicknesses are varied symmetrically between pressure and suction side of the blade.
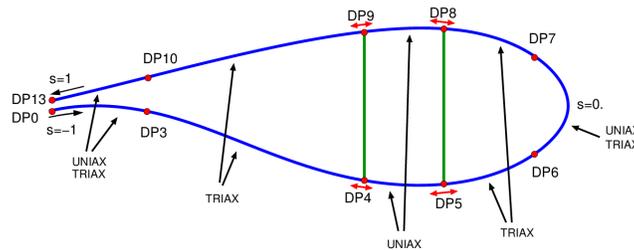

Figure 2. Region division points (DP) definition: red points indicate division points between regions; their positions are defined as curve fraction from pressure side TE (s=-1) to LE (s=0) to suction side TE (s=1).
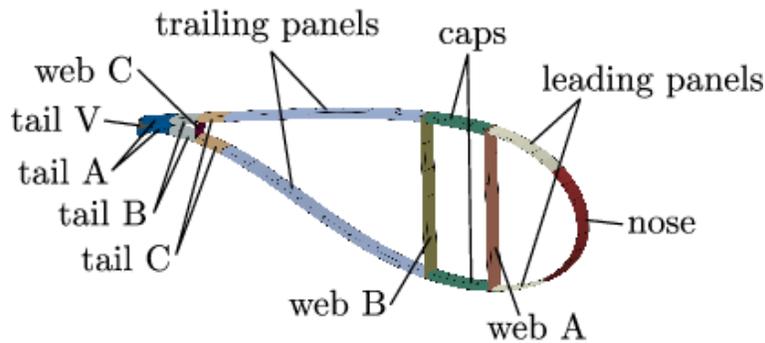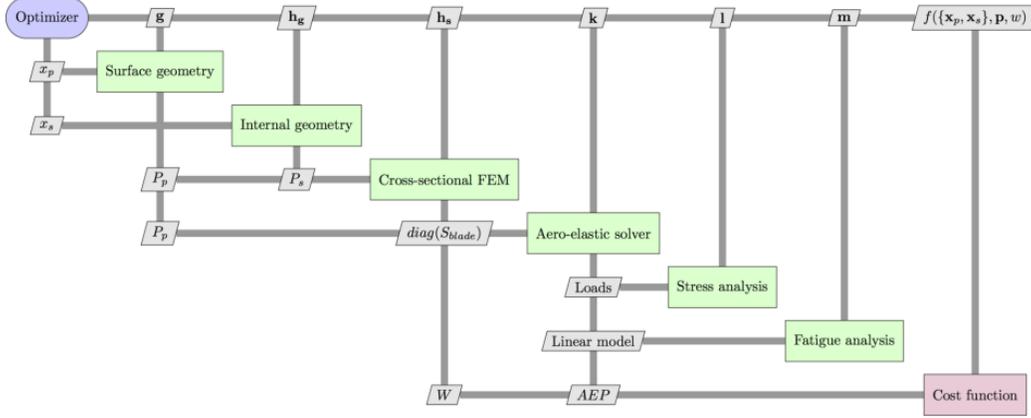

Figure 3. Blade section internal structure layup

American Institute of Aeronautics and Astronautics

Figure 4. **Extended design structure matrix diagram of the workflow in HawtOpt2**

IV.   Problem definition

The numerical optimization problem that is solved is defined as:

$$
\begin{aligned}
\underset{\mathbf{x}_p, \mathbf{x}_s}{\text{minimize}} \quad & f(\{\mathbf{x}_p, \mathbf{x}_s\}, \mathbf{p}, w) \\
\text{subject to} \quad & \mathbf{g}(\mathbf{x}_p) \leq \mathbf{0}, \\
& \mathbf{h_g}(\mathbf{x}_s) \leq \mathbf{0}, \\
& \mathbf{h_s}(\mathbf{x}_s) \leq \mathbf{0}, \\
& \mathbf{k}(\{\mathbf{x}_p, \mathbf{x}_s\}) \leq \mathbf{0}
\end{aligned}
\tag{1}
$$

A scalar cost function f is minimized, subject to several nonlinear constraints. The cost function depends on a set of planform $\mathbf{x}_p$ and structural $\mathbf{x}_p$ design variables, a set of constant parameters p, and a weight w. The planform variables define the outer shape of the blade. These variables are the chord, the twist, and the relative thickness distributions. The structural variables define the internal geometry of each blade section. These variables include thicknesses of the different material layups and position and width of the spar caps.

The cost function is defined as:

$$
f(\{\mathbf{x}_p, \mathbf{x}_s\}, \mathbf{p}, w) = (1 - w) \frac{W(\{\mathbf{x}_p, \mathbf{x}_s\}, \mathbf{p})}{W(\{\mathbf{0}, \mathbf{0}\}, \mathbf{p})} + w \frac{AEP(\{\mathbf{0}, \mathbf{0}\}, \mathbf{p})}{AEP(\{\mathbf{x}_p, \mathbf{x}_s\}, \mathbf{p})}
\tag{2}
$$

where W is the blade weight, AEP is the annual energy production. $W(\{\mathbf{0}, \mathbf{0}\}, \mathbf{p})$ and $AEP(\{\mathbf{0}, \mathbf{0}\}, \mathbf{p})$ are the blade weight and annual energy production of the baseline design.

Three different type of constraints are defined depending on the variables they depend on:

- Constraints $\mathbf{g}$ depend only on planform parameters;

- Constraints $\mathbf{h_g}$ depend only on structural parameters;

- Constraints $\mathbf{h_s}$ denote the limits on the maximum allowable stresses in the structure;

- Constraints $\mathbf{k}$ depend on both the planform and structural variables.

Figure 4 shows a so-called extended design structure matrix diagram of the workflow in HawtOpt2.

The planform design variables include the parametrized distributions of chord, twist, relative thickness, and pitch axis aft leading edge. The structural design variables include the position and thickness of regions that each cover a fraction of the cross-sectional layup. As described above, only the rotor is optimized in this work leaving all other parameters unaltered. Although the outer shape is controlled by the optimizer, the cross sectional shape is based on an interpolation between the FFA-W3 airfoil series, and as such, the aerodynamic characteristics along the blade are approximated by linear interpolation of the base airfoils, which is common practice in most aeroelastic solvers.
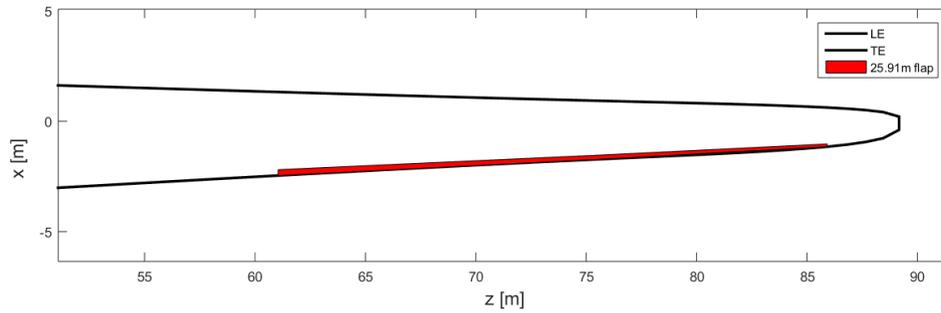
Figure 5. Flap geometry implemented on the planform of the baseline DTU 10MW RWT blade.

Table 1 summarizes all the design variables included in the optimizations problems. Table 2 lists all the constraint considered in the optimizations.

The effect of the trailing edge flaps, apart from the fatigue load reduction, is taken into account also in the cross sectional geometry details, by incorporating material definition corresponding to a polymer based design as used in.[6]

The simulated flap configuration is chosen based on prior studies. The flap extent on the baseline blade planform is shown in Figure 5. The flap extends on 30% of the blade span with a constant 10% chordwise length.

American Institute of Aeronautics and Astronautics

Table 1. Free form deformation spline (FFD) design variables used in the optimizations.

Parameter	Spanwise distribution	# of DVs	Comment
Chord	[(0, 0.1), (0.1, 0.2), 0.5, 0.85, 1.0]	5	Tip chord fixed, inner sections grouped
Twist	[(0, 0.1), 0.2, 0.5, 0.85, 1.0]	5	Root twist fixed, inner sections grouped
Relative thickness	[0.1, 0.2, 0.5, 0.85]	4	Root and tip thickness fixed
Trailing panel triax	[0, 0.1, 0.2, 0.5, 0.85, 1.0]	6	Pressure/suction side
Spar cap uniax	[0, 0.1, 0.2, 0.5, 0.85, 1.0]	6	Pressure/suction side
Leading edge uniax	[0, 0.1, 0.2, 0.5, 0.85, 1.0]	6	Pressure/suction side
Leading edge and leading panel triax	[0, 0.1, 0.2, 0.5, 0.85, 1.0]	6	Pressure/suction side
DP4	[(0, .1), 0.2, 0.5, 0.85]	4	Inner CPs grouped
DP5	[(0, .1), 0.2, 0.5, 0.85]	4	Inner CPs grouped
DP8	[(0, .1), 0.2, 0.5, 0.85]	4	Inner CPs grouped
DP9	[(0, .1), 0.2, 0.5, 0.85]	4	Inner CPs grouped
Total		54	

Table 2. Non-linear constraints used in the optimizations.

Constraint	Value	# of Cons.	Comment
max(chord)	< 6.2 m	1	Maximum chord limited for transport.
min(relative thickness)	> 0.24	1	Same airfoil series as used on the DTU 10MW RWT.
min(material thickness)	> 0.0	19	Ensure FFD splines do not produce negative thickness.
$t/w_{sparcap}$	> 0.08	38	Basic constraint to avoid spar cap buckling.
max(Flapwise tip deflection)	< ref value	1	Operational tip deflection cannot exceed that of the DTU 10MW RWT.
max(Flapwise tip deflection)	< ref value	1	Extreme wind standstill tip deflection cannot exceed that of the DTU 10MW RWT.
max(Edgewise tip deflection)	< ref value	1	Extreme wind standstill tip deflection cannot exceed that of the DTU 10MW RWT.
Rotor thrust	< ref value	1	Operational rotor thrust cannot exceed that of the DTU 10MW RWT.
Blade flapwise load	< ref value	1	Extreme wind standstill loads cannot exceed that of the DTU 10MW RWT.
Blade edgewise load	< ref value	1	Extreme wind standstill loads cannot exceed that of the DTU 10MW RWT.
Lift coefficient @$r/R = [0.5-1]$	< 1.35	15	Limit operational lift coefficient to avoid stall.
Ultimate strain criteria	< 1.0	180	Material failure in each section for six load cases.
Trailing edge thickness ratio	< 1.0	57	Ensure that material thickness does not exceed trailing edge thickness.
Blade root flapwise fatigue	< 10%	2	Fatigue reduction at 12 and 18 m/s.
Total		319	

V.   Results

Six different models are compared:

- *DTU 10MW*;

- *DTU 10MW with flaps*;

- *Baseline*: DTU 10MW optimized for AEP/weight, it represents the optimization baseline;

- *Flaps*: baseline design with flaps geometry optimized for AEP/weight;

- *Baseline+Fatigue*: baseline design optimized for AEP/weight with fatigue reduction constraint;

- *Flaps+Fatigue*: baseline design with flaps geometry optimized for AEP/weight with fatigue reduction constraint.

The initial design for the optimizations without flaps is the standard design of the DTU 10MW Reference Wind Turbine.[31] The optimization including flaps have a different initial design based on the DTU 10MW RWT but incorporating the flap material definition for the trailing edge regions where the flaps are placed. This model is obtained by simply substituting the original material with the rubber used for the flaps in the regions where the flaps are located. Figure 6 shows the material distribution at the trailing edge of the baseline model and the baseline model with flaps. The material distributions of the two models are identical except for outer 30% of the blade where all the glassfiber materials are substituted by thermoplastic polymer (in the figure refered to as "rubber"). The thicknesses of the materials in the trailing edge region are not included as optimization variables, as indicated in Table 1, therefore there is no difference in the trailing edge layups between the optimized models and the references.

In all the optimization cases, the cost function is a compound objective consisting of both mass and AEP as defined in Eq. 2 where the weight w is defined as $w=0.925$.

Case *Baseline+Fatigue* and *Flaps+Fatigue* differ from *Baseline* and *Flaps* on an additional constraint on the fatigue damage of the blade root flapwise bending moment. The constraint imposes a fatigue reduction of 10% compared to the corresponding initial design. The fatigue is estimated based on a spectral method and a linear model computed with HAWCStab2. The linear model is in closed-loop configuration and therefore includes the wind turbine controller. For this investigation the tuning of the controller is kept constant throughout the entire optimization.

The constraints on the loads and on the tip deflections are set such that the values of the *DTU 10MW* model are not exceeded. Therefore they all satisfy the same tip deflection, max thrust, max hub loads, and max blade loads. This is done to guarantee that potentially all the blades could be installed on the same wind turbine.
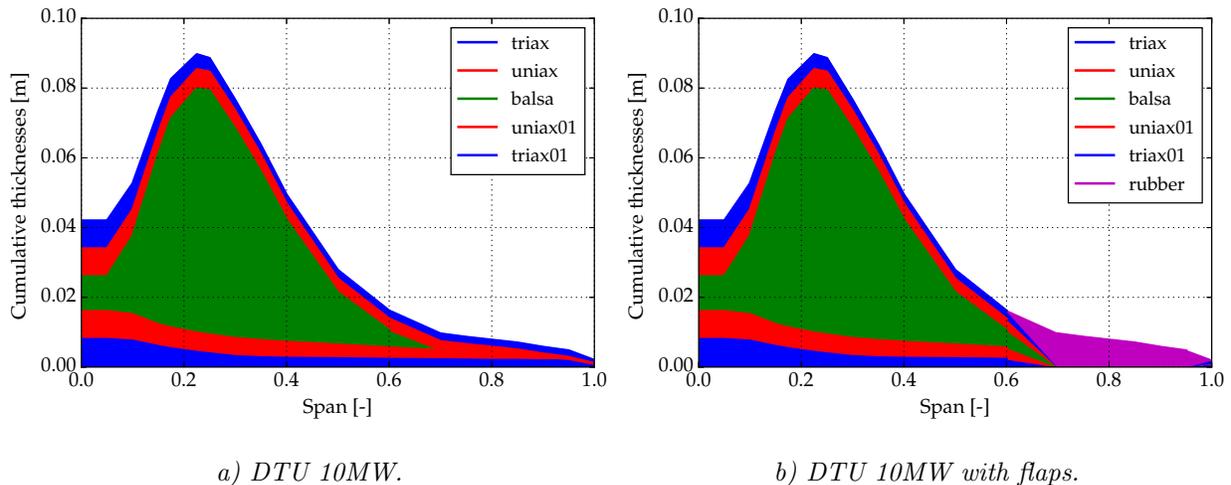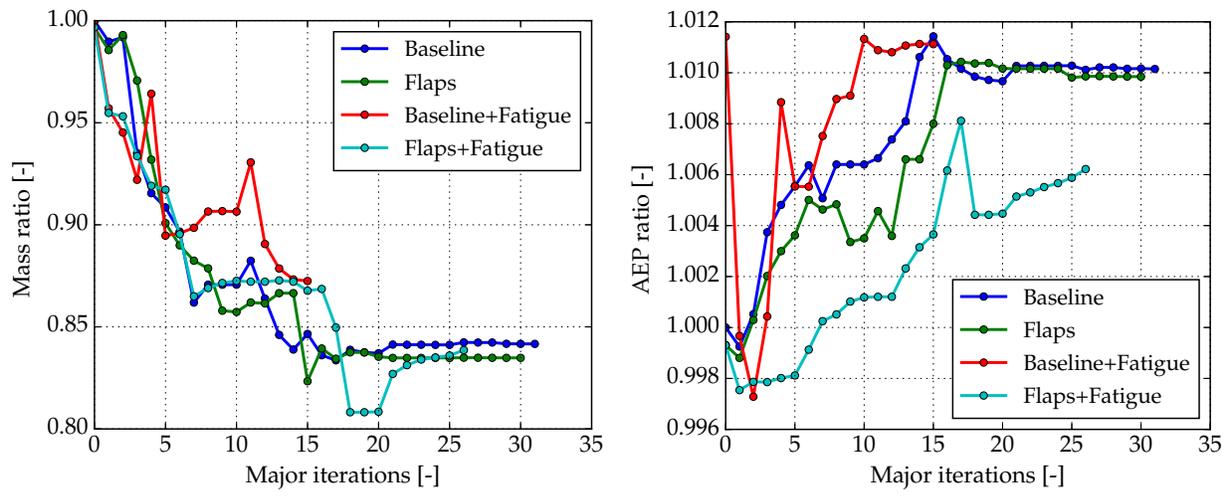

a) DTU 10MW.

b) DTU 10MW with flaps.

Figure 6. Comparison of the spanwise layups material distribution at the trailing edge between the baseline model and the baseline with flaps model.

American Institute of Aeronautics and Astronautics

a) Blade mass ratio.　　　　　　　　　　　　　　　　b) AEP ratio.

Figure 7. Blade mass and annual energy production ratios at each major iterations of the optimizations. Ratios obtained by normalizing with respect to the respective values of the *DTU 10MW* model. Comparison between baseline design, design with flap geometry, baseline design with fatigue constraint, and design with active flap geometry and fatigue constraint.

Figure 7 shows the evolution of the blade mass ratio and of the AEP ratio during the optimization procedure at each major iteration for the four optimized models. All the optimization runs were manually stopped before the algorithm could reach a stopping criteria due to time considerations. The two cases without fatigue could run for more iterations than the cases with the fatigue indeed they show small mass and AEP variations in the last few iterations. Models *Baseline+Fatigue* and *Flaps+Fatigue* are clearly still far from being converged, however, at the iteration they were stopped, the constraints were violated only by a small percentage. All the cases, except for *Baseline+Fatigue*, reach a blade mass reduction of approximately 16%. On the other hand the AEP is increased by 1% for all the cases but for *Flaps+Fatigue*. The designs that include the flaps geometry are clearly not penalized compared to the standard ones. This similar behavior is an indication that, for the considered problem, the loss in stiffness that is introduced by removing load-carrying materials at the trailing edge to make space to for the flaps is not compromising the design.

Figure 8 shows the variations of the fatigue constraint for models *Baseline+Fatigue* and *Flaps+Fatigue* for each major iteration. The constraint is violated by 10% at the initial design because it is set to be reduced by 10% with respect to the initial value. The model with flaps has already a lower initial fatigue value due to
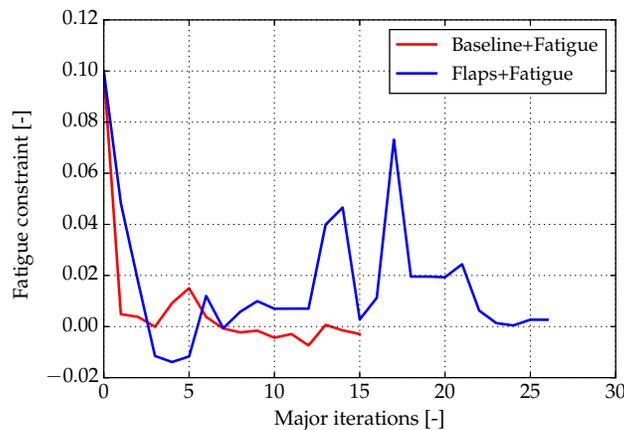

Figure 8. Variations of the fatigue constraint at each major iteration. Comparison of the baseline design and the design with flaps. Positive values indicate that the constraint is violated.

American Institute of Aeronautics and Astronautics

the effect of the flaps themselves. Within few iterations the constraints are significantly reduced. However, model *Flaps+Fatigue* has to compromise more on the value of the constraint to satisfy other constraints and reduce the objective function.

Figure 9 shows a comparison of chord, relative thickness, mass, and flapwise, edgewise, and torsional stiffness distribution between all the optimized models, *Baseline*, *Flaps*, *Baseline+Fatigue*, and *Flaps+Fatigue*, and the *DTU 10MW* model. All the optimized models have a lower chord distribution compared to the initial design. The chord is reduced significantly at the blade root to reduce blade mass and in the outer part of the blade to reduce the thrust and therefore tip displacement. The relative thickness decreases in the first $30m$ of the blade to gain aerodynamic performances. On the other hand in the central part it increases to allow to keep the stiffness high when the chord is reduced to decrease the aerodynamic thrust. The mass distribution decreases in all the cases significantly in the first half of the blade and it slightly increases for all the model but *Flaps* in the outer $40m$. All the stiffnesses decreases significantly at the root due to the large change in the chord. Flapwise stiffnesses are increased in the outer part of the blade in all the cases but for *Flaps*. The distribution of edgewise stiffness clearly shows a significant reduction in the outer part of the blade for the models with the flaps. The reduction is due to the lower structural properties of the rubber material used for the flaps compared to the glassfiber.

Table3 shows the variations of blade mass, AEP, and lifetime blade root flapwise fatigue damage. The AEP and the fatigue are obtained from nonlinear time marching simulations evaluated with HAWC2.[33] The values are obtained from DLC1.2 of the design load basis described in[32] that comprehends 216 simulations. The mass and AEP changes on average confirm the ones obtained using the models of the optimization
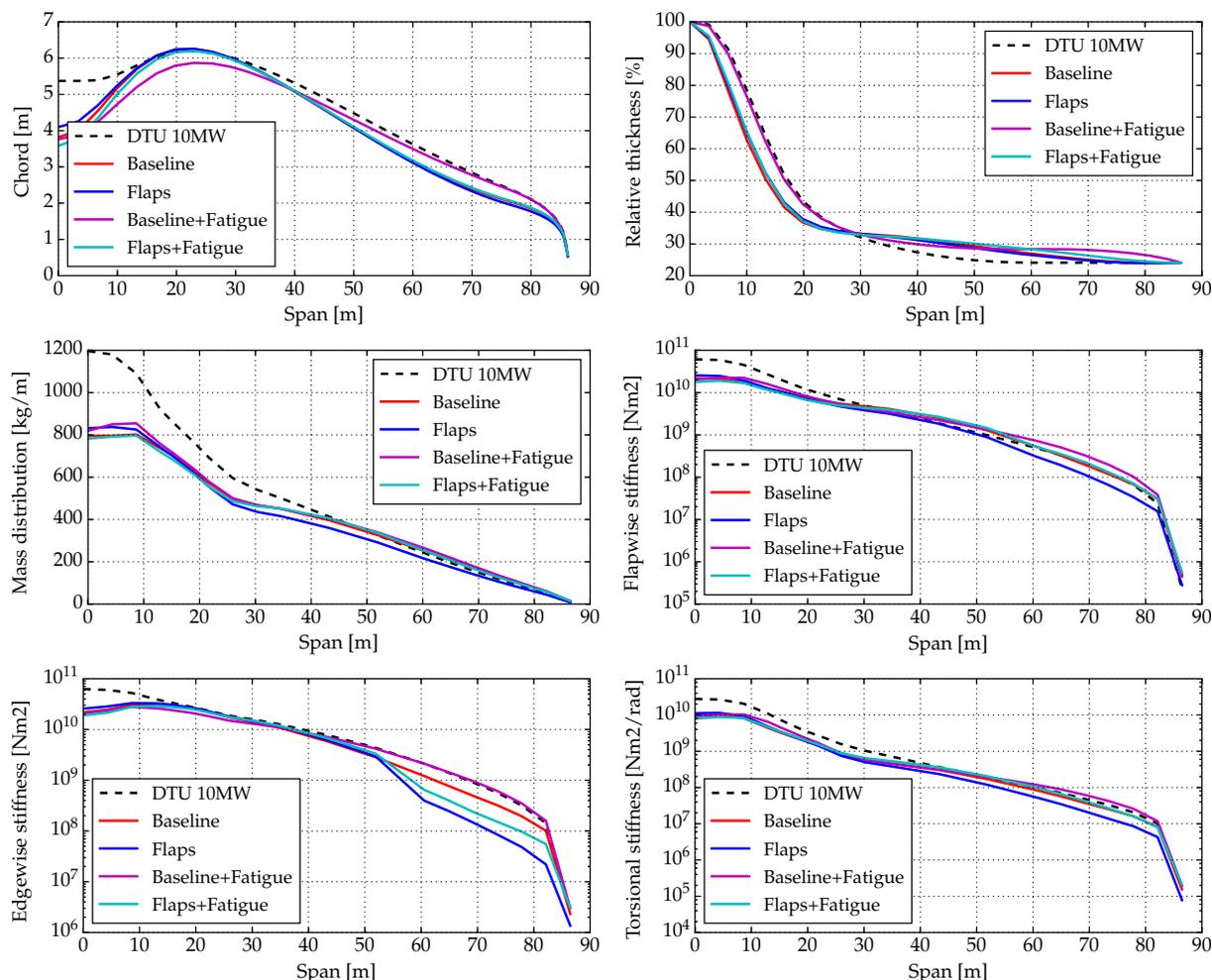

Figure 9. Comparison of chord, relative thickness, mass, and stiffnesses distributions between the optimized models and the *DTU 10MW*.

American Institute of Aeronautics and Astronautics

framework. The blade root flapwise moment fatigue results suggest that a blade design optimized for reduced mass also shows a benefit in reduced fatigue, but this potential is almost double when the fatigue constraint is used in the optimization. Furthermore, a blade design optimized for flap geometry shows almost double the fatigue reduction potential compared to the original blade when flaps are used actively in both designs. This potential is not further increased when the blade design with the fatigue constraint is evaluated with active flaps.

VI.   Conclusion

In the application of the described optimization framework both outer shape and internal structure are optimized for achieving both a reduction in mass as well as an increase in AEP, which are conflicting objectives. Furthermore it is shown that considerable AEP increase /weight reduction gain together with a fatigue load reduction is achieved with the additional use of active flaps. However, the fatigue constraint limits the blade mass reduction compared to the unconstrained case, and it leads to different AEP levels. The evaluation of the optimized blade designs with active flaps in non-linear time domain simulations shows that that the blade fatigue load reduction potential is further enhanced when blade designs incorporating the flap geometry are utilized.

Acknowledgments

References

[1]Barlas, T. K., Van Kuik, G. A. M., *Review of state of the art in smart rotor control research for wind turbines*, Progress in Aerospace Sciences, 46(1), 1-27, 2010.

[2]Van Wingerden, J., Hulskamp, A., Barlas, T., Houtzager, I., Bersee, H., van Kuik, G., and Verhaegen, M., *Two-degree-of-freedom active vibration control of a prototyped 'smart' rotor*. Control Systems Technology, IEEE Transactions on, 19(2), 284-296, 2011.

[3]Castaignet, D., Barlas, T., Buhl, T., Poulsen, N. K., Wedel-Heinen, J. J., Olesen, N. A., Bak, C., and Kim, T., *Full-scale test of trailing edge flaps on a Vestas V27 wind turbine: active load reduction and system identification*. Wind Energy, 17(4), 549-564, 2014.

[4]Barlas, T., *Active aerodynamic load control on wind turbine blades: Aeroservoelastic modelling and wind tunnel experiments*, PhD thesis, TUDelft, 2011.

[5]Madsen HA., Andersen P. B., Andersen T., Bak C. and Buhl T., *The potentials of the controllable rubber trailing edge flap (CRTEF)*. Proceedings of EWEC 2010, 20-23 April 2010, Warsaw, Poland

[6]Madsen HA., et. al., *Towards an industrial manufactured morphing trailing edge flap system for wind turbines*. Proceedings of EWEC 2014, Barcelona, Spain.

[7]Barlas, T. K. and Madsen, H. A., *Influence of Actuator Dynamics on the Load Reduction Poetntial of Wind Turbines with Distributed Controllable Rubber Trailing Edge Flaps (CRTEF)*. Proceedings of ICAST2011: 22nd International Conference on Adaptive Structures and Technologies, October 10-12, 2011, Corfu, Greece.

[8]Bergami, L., *Adaptive Trailing Edge Flaps for Active Load Alleviation in a Smart Rotor Configuration*, PhD thesis, DTU Wind Energy, 2013.

[9]Fuglsang, P., Bak, C., Schepers, J. G., Bulder, B., Cockerill, T. T., Claiden, P., Olesen, A., and van Rossen, R., *Site-specific Design Optimization of Wind Turbines*, Wind Energy, 5(4), 261-279, 2002.

Table 3. **Variations of blade mass, AEP and blade root flapwise moment fatigue with respect to the *DTU 10MW* design. Negative values indicate reductions. Values obtained from HAWC2 simulations.**

	Blade mass [%]	AEP [%]	Lifetime blade root flapwise fatigue [%]
DTU 10MW with flaps	-0.3	0.21	-12.1
Baseline	-15.8	-0.05	-5.6
Flaps	-19.6	0.51	-23.1
Baseline+Fatigue	-13.2	-0.08	-8.9
Flaps+Fatigue	-16.4	0.79	-21.8

[10]Bottasso, C. L., Campagnolo, F., and Croce, A., *Multi-disciplinary constrained optimization of wind turbines*, Multibody System Dynamics, 27(1), 21-53, 2012.

[11]Ashuri, T., Zaaijer, M. B., Martins, J. R. R. A., van Bussel, G. J. W., and van Kuik, G. A. M., *Multidisciplinary design optimization of offshore wind turbines for minimum levelized cost of energy*, Renewable Energy, 68, 893-905, 2014.

[12]Merz, K. O., *Rapid optimization of stall-regulated wind turbine blades using a frequency-domain method: Part 1, loads analysis*, Wind Energy, 2014.

[13]Merz, K. O., *Rapid optimization of stall-regulated wind turbine blades using a frequency-domain method: Part 2, cost function selection and results*, Wind Energy, 2014.

[14]Fischer, G. R., Kipouros, T., and Savill, A. M., *Multi-objective optimisation of horizontal axis wind turbine structure and energy production using aerofoil and blade properties as design variables*, Renewable Energy, 62(0), 506-515, 2014.

[15]Ning, S. A., Damiani, R., and Moriarty, P. J., *Objectives and Constraints for Wind Turbine Optimization*, Journal of Solar Energy Engineering, 136(4), 041010, 2014.

[16]Zahle, F., Tibaldi, C., Verelst, D. R., Bak, C., Bitche, R., and Blasques, J. P. A. A., *Aero-Elastic Optimization of a 10 MW Wind Turbine*, Proceedings of the 33rd Wind Energy Symposium , Kissimmee, Florida, U.S.A., 2015.

[17]Tibaldi, C., *Concurrent Aeroservoelastic Design and Optimization of Wind Turbines*, PhD Thesis, DTU Wind Energy, 2015.

[18]Tibaldi C., Henriksen L., Hansen M.H., Bak C., *Wind turbine fatigue damage evaluation based on a linear model and a spectral method.* Wind Energy, 2015. doi: 10.1002/we.1898.

[19]http://openmdao.org

[20]Gill PE, Murray W, Saunders MA. *SNOPT: An SQP algorithm for large-scale constrained optimization (reprinted from SIAM journal optimization, vol 12, pg 979-1006, 2002).* Siam Review 2005; **47**(1):99–131,

[21]Gill PE, Murray W, Saunders MA. *SNOPT 7 user's guide.* Technical Report Numerical Analysis Report NA 04-1, Department of Mathematics, University of California, 2008.

[22]http://fusedwind.org

[23]Blasques, P., *User s Manual for BECAS A cross section analysis tool for anisotropic and inhomogeneous beam sections of arbitrary geometry*, 2012.

[24]Blasques, J. P. and Stolpe, M., *Multi-material topology optimization of laminated composite beam cross sections*, Composite Structures,94(11), 3278-3289, 2012.

[25]http://becas.dtu.dk

[26]http://hawcstab2.vindenergi.dtu.dk

[27]Hansen, M. H., *Aeroelastic stability analysis of wind turbines using an eigenvalue approach.* Wind Energy, 7(2), 133-143, 2004.

[28]Hansen, M. H., *Aeroelastic Properties of Backward Swept Blades* American Institute of Aeronautics and Astronautics, Orlando, Florida, 1-19, 2011.

[29]Sønderby, I. and Hansen, M. H., *Open-loop frequency response analysis of a wind turbine using a high-order linear aeroelastic model*, Wind Energy, 17(8), 1147-1167, 2014.

[30]Bergami, L. and Hansen, M. H., *A Linear Time Invariant Model of a Smart Rotor with Adaptive Trailing Edge Flaps*, Wind Energy, to appear.

[31]Bak, C. et al., *Description of the DTU 10 MW Reference Wind Turbine*, DTU Wind Energy Report-I-0092, 2013.

[32]Hansen, M. H. et al., *Design Load Basis for onshore turbines*, DTU Wind Energy Report-E-0179, 2015.

[33]Larsen, T. J. et al., *How 2 Hawc2, the user's manual*, Risø Report-R-1579(ver. 4.4)(EN), 2013..